AGU ADVANCING EARTH AND SPACE SCIENCE

Geophysical Research Letters

RESEARCH LETTER
10.1029/2020GL091048

New Results on the Direct Observations of Thermal Radio Emission from a Solar Coronal Mass Ejection

R. Ramesh[1], A. Kumari[1,2], C. Kathiravan[1], D. Ketaki[1,3], and T. J. Wang[4,5]

[1]Radio Astronomy Group, Indian Institute of Astrophysics, Bangalore, Karnataka, India, [2]Department of Physics, University of Helsinki, Helsinki, Finland, [3]Department of Physics, Sir Parashurambhau College, Pune, Maharashtra, India, [4]Department of Physics, The Catholic University of America, Washington, DC,, USA, [5]NASA Goddard Space Flight Center, Greenbelt, MD, USA

Key Points:

- We report observations of thermal radio emission from the frontal structure of a coronal mass ejection (CME) simultaneously at 80 and 53 MHz
- The electron density, mass, and magnetic field of the CME were estimated directly from the observed thermal radio emission
- Similar observations with larger low-frequency radio antenna arrays like LOFAR and Square Kilometre (SKA) are expected to be useful to understand CMEs

Correspondence to:
R. Ramesh,
ramesh@iiap.res.in

Citation:
Ramesh, R., Kumari, A., Kathiravan, C., Ketaki, D., & Wang, T. J. (2021). New results on the direct observations of thermal radio emission from a solar coronal mass ejection. *Geophysical Research Letters*, *48*, e2020GL091048. https://doi.org/10.1029/2020GL091048

Received 29 SEP 2020
Accepted 5 MAR 2021

Abstract We report observations of thermal emission from the frontal structure of a coronal mass ejection (CME) using data obtained with the Gauribidanur RAdioheliograPH simultaneously at 80 and 53 MHz on May 1, 2016. The CME was due to activity on the far side of the Sun, but near its limb. No nonthermal radio burst activity was noticed. This provided an opportunity to observe the faint thermal radio emission from the CME, and hence directly estimate the electron density, mass, and magnetic field strength of the plasma entrained in the CME. Considering that CMEs are mostly observed only in whitelight and reports on their plasma characteristics are also limited, the rare direct radio observations of thermal emission from a CME and independent diagnosis of its plasma parameters are important measurements in the field of CME physics.

Plain Language Summary Near-Sun observations of coronal mass ejections (CMEs) in white light are difficult with the existing coronagraphs due to the large size of their occulting disks. Furthermore the observations are limited to the corona off the solar limb since the occulting disks cover the corona overlying the solar disk. Radio observations are useful in this connection since there are no occulting disks. So both disk as well as limb corona can be simultaneously observed. Additionally, it is easier to carry out polarization studies and also calibrate the data using observations of other cosmic radio sources.

1. Introduction

Coronal mass ejections (CMEs) are large-scale and energetic eruptions in the solar atmosphere during which $\approx 10^{12}$–10^{16}g of magnetized coronal plasma are ejected into the heliosphere at speeds ranging from ≈ 100 to 3,000 km/s (e.g., Vourlidas et al., 2010). They are mostly observed in whitelight using coronagraphs which use an occulter to block the bright light from the solar photosphere so that structures like CMEs can be observed with better contrast. But the size of the coronagraph occulters to date has always been larger than that of the photosphere. For example, in the *Large Angle and Spectrometric Coronagraph C2* (LASCO C2, Brueckner et al., 1995) on board the *Solar and Heliospheric Observatory* (SOHO), the occulter covers a heliocentric distance (r) of ≈ 2.2 $R_\odot$, where $R_\odot$ is the radius of the photosphere. This prevents observations of the corona present immediately off the solar limb, in addition to the corona above the solar disk. Radio observations are unique in this connection since there is no occulter. The radio emission associated with and/or from the CMEs can be divided into two classes, thermal and nonthermal (e.g., Vourlidas, 2004). In the nonthermal case, type IV radio bursts due to gyrosynchrotron and/or plasma emission from the electrons in the CME (Bain et al., 2014; Bastian et al., 2001; Carley et al., 2017; Gary et al., 1985; Gopalswamy & Kundu, 1987, 1989, 1990; Hariharan, Ramesh, Kathiravan, & Wang, 2016; Maia et al., 2007; Mondal et al., 2020; Morosan et al., 2019; Ramesh et al., 2013; Sasikumar Raja et al., 2014; Stewart et al., 1974; Tun & Vourlidas, 2013; Vasanth et al., 2019; Wagner et al., 1981), type II radio bursts due to plasma emission from the electrons accelerated by MHD shocks driven by the CME (Aurass, 1997; Chrysaphi et al., 2018; Gopalswamy, 2006; Kumari et al., 2017, 2017b, 2019; Maguire et al., 2020; Mann et al., 1995; Ebenezer et al., 2001b; Ramesh et al, 2010b, 2012a; Stewart et al., 1974), and type I noise storm continuum due to plasma emission from changes in the coronal magnetic field during a CME (Kathiravan et al., 2007; Kerdraon et al., 1983; Ramesh & Sundaram, 2000a) have been widely reported. Compared to this, there are only a few reports of direct detection of CMEs at radio frequencies via thermal bremsstrahlung emission (Gopalswamy & Kundu, 1992, 1993; Kathiravan et al., 2002; Kathiravan & Ramesh, 2004, 2005; Ramesh, 2005a; Ramesh

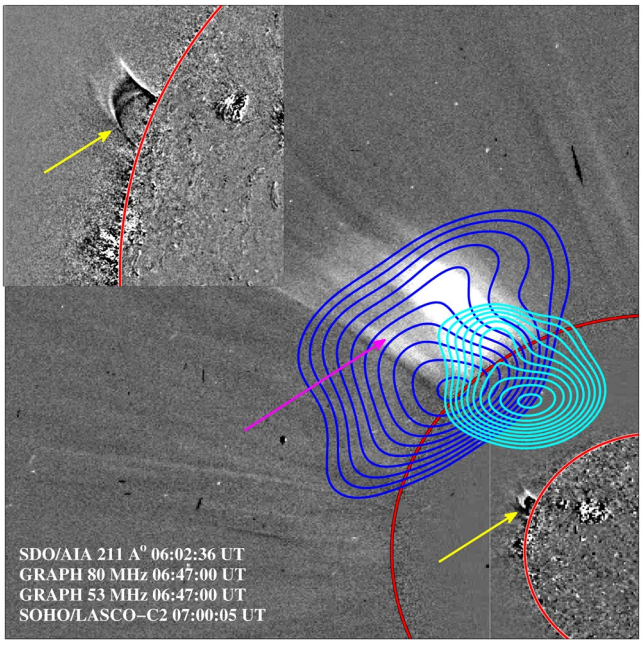

Figure 1. A composite of the difference images obtained using EUV (≈06:02–05:41 UT), radio (≈06:47–06:42 UT), and whitelight (≈07:00–06:00 UT) observations on May 1, 2016. The inner and outer "red" circles indicate the solar limb (radius ≈ $1R_{\odot}$), and the occulter in the SOHO/LASCO-C2 coronagraph (radius ≈ 2.2 $R_{\odot}$). The bright emission above the occulter (indicated by "magenta" arrow) is the whitelight CME. The inset in the upper left corner is a close-up view of the region indicated by the "yellow" arrow on the SDO/AIA-211 Å image. The "cyan" and "blue" contours correspond to radio observations at 80 and 53 MHz. The contour levels are ≈ [63, 67, 71, 75, 79, 83, 87, 91, 95, 99]% of 3.4×10^5K (80 MHz) and 0.8×10^5K (53 MHz).

et al., 2003; Sheridan et al., 1978). Here we present radio observations of thermal emission from a CME simultaneously at two different frequencies and compare the nature of the observed emission with published reports. We were fortunate that there was no flare activity seen on the visible hemisphere of the Sun whose associated nonthermal radio burst activity would have otherwise probably prevented us from observing the comparatively weak thermal radio emission from the CME (e.g., Bastian & Gary, 1997). For example, the peak flux density of the radio burst observed on December 6, 2006 was ≈ 10^6sfu (sfu = solar flux unit = 10^{-22} W/m^2/Hz) in the 1–2 GHz frequency range (Gary, 2019). Compared to this the flux density of thermal radio emission from the "quiet" Sun is ∼few sfu or even less. This calls for a very large dynamic range to observe the radio burst and the "quiet" Sun simultaneously.

2. Observations

The radio observations were carried out on May 1, 2016 using the different facilities in Gauribidanur Observatory (https://www.iiap.res.in/?q=centers/radio, Ramesh, 2011a, 2014). Two-dimensional images obtained with the *Gauribidanur RAdioheliograPH* (GRAPH [Ramesh et al., 1998, 1999b, 2006b]) at 80 and 53 MHz were used to obtain positional information. The observations were carried out close to the local meridian transit time of the Sun (≈06:30 UT). For radio spectral data, we used observations with the *Gauribidanur LOw-frequency Solar Spectrograph* (GLOSS; Ebenezer et al., 2001a, 2007; Kishore et al., 2014; Hariharan, Ramesh, Kathiravan, Abhilash, & Rajalingam, 2016), *Gauribidanur RAdio Spectro-Polarimeter* (GRASP, Hariharan et al., 2015; Kishore et al., 2015; Sasikumar Raja et al., 2013), and e-CALLISTO (Benz et al., 2009; Monstein et al., 2007). We also used data obtained with the Gauribidanur Radio Interferometric Polarimeter (GRIP, Ramesh & Sastry, 2005b; Ramesh et al., 2008). The combined use of the aforementioned observations helps to understand the radio signatures associated with the corresponding solar activity in a better manner (e.g., Sasikumar Raja & Ramesh, 2013). Observations in EUV at 211 Å with the *Atmospheric Imaging Assembly* (AIA, Lemen et al., 2012) onboard the *Solar Dynamics Observatory* (SDO), and in whitelight with the COR1 coronoagraph of the *Sun-Earth Connection Coronal and Heliospheric Investigation* (SECCHI, Howard et al., 2008) on board the *Solar TErrestrial RElationship Observatory* (STEREO) and SOHO/LASCO were used to supplement the radio observations.

Figure 1 shows a composite of the difference images obtained in EUV, whitelight, and radio on May 1, 2016 during the interval ≈ 6–7 UT. An inspection of the SOHO/LASCO CME catalog (https://cdaw.gsfc.nasa.gov/CME_list/UNIVERSAL/2016_05/univ2016_05.html) indicates that close to the above epoch a CME was observed around position angle (PA, measured counter clockwise from the solar north) ≈ 50°. The enhanced whitelight emission in Figure 1 corresponds to the frontal structure of the aforementioned CME. It was a narrow CME without the three-part structure associated with a typical CME. No streamer-blowout was also noticed (https://lasco-www.nrl.navy.mil/carr_maps/c2/). Its various characteristics estimated from the SOHO-LASCO observations are, angular width ≈ 36°; linear speed in the plane-of-sky ≈ 482 km/s; acceleration ≈ −10 m/s^2; mass ≈ 1.2×10^{15}g; kinetic energy ≈ 1.4×10^{30} erg. An inspection of the SDO/AIA-211 Å data indicates that the CME was most likely due to activity in the sunspot region AR12541 located at ≈ N01E94 (https://www.lmsal.com/solarsoft/ssw/last_events-2016/last_events_20160503_1121/index.html). Since the region was just behind the limb, any projection effects on the aforementioned CME parameters will be very minimal. We verified the activity in AR12541 using STEREO-A/EUVI 195 Å difference images. STEREO-A was at ≈ *E*160° during the above period (https://stereo-ssc.nascom.nasa.gov/cgi-bin/make_where_gif). This implies that AR12541 was located at ≈24° inside the limb for STEREO-A view (see Figures 2a–2c).

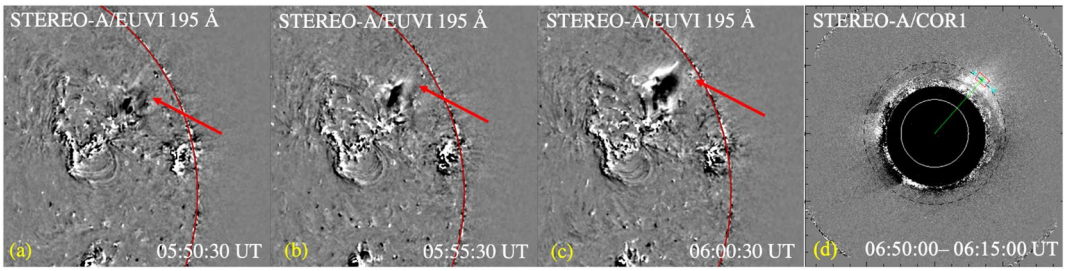

Figure 2. Panels (a–c) are the STEREO-A/EUVI 195 Å running difference images of activity in AR12541 (indicated by "red" arrow) on May 1, 2016. The "red" circle indicates the solar limb. Panel (d) is the STEREO-A/COR1 pB difference image obtained on the same day. The "white" and "black" circles indicate the solar limb and the coronagraph occulter (radius ≈ 1.4 $R_\odot$), respectively. The enhanced emission to the upper right of the occulter corresponds to the same CME shown in Figure 1. Its electron density (N_e^{cor1a}) was estimated from the region covered by the "red" box.

The GRAPH observations shown in Figure 1 are close to ≈ 06:47 UT at 53 and 80 MHz simultaneously. The spatio-temporal correspondence between the radio contours and the whitelight CME indicates that the radio emission could be due to the CME. The larger size of the radio contours, particularly at 53 MHz and in the north-south direction, is likely due to the comparatively limited angular resolution of GRAPH (≈ 4 × 6′ (R.A. × decl.) and ≈ 6 × 9′ at 80 and 53 MHz, respectively.) The EUV eruptive activity noticed near the solar limb indicates the source region and the early phase of the CME. Though it appears that the EUV eruption is slightly displaced from the whitelight and radio structures, an inspection of the 12 s running difference images using SDO/AIA-211 Å and SDO/AIA-193 Å indicate that the eruptive activity rises up nonradially in the direction toward the locations of the whitelight and radio structures at a later time.

The centroids of the radio emission shown in Figure 1 are located at $r_{80} \approx 1.7 \pm 0.2\ R_\odot$ (80 MHz) and $r_{53} \approx 2.1 \pm 0.2\ R_\odot$ (53 MHz). Any possible error in the position of the centroids due to propagation effects such as scattering by density inhomogeneities in the solar corona and/or refraction in the Earth's ionosphere is expected to be within the above error limit (Kathiravan et al., 2011; Mugundhan et al., 2016, 2018a; Ramesh et al., 1999a, 2012b; Stewart & McLean, 1982). The fact that the Sun is presently going through a period of extended minimum (during which the observations reported in the present work were carried out) indicates that the effects of scattering are likely to be less pronounced (Mugundhan et al., 2017; Ramesh et al., 2020; Sasikumar Raja et al., 2016). Furthermore, the observations were carried out close to the local noon during which time the zenith angle of the Sun is the least. Possible positional shifts in hour angle and declination due to ionospheric effects are expected to be negligible during that time. Note that the elevation of Sun on May 1, 2016 when the present observations were carried out was ≈ 88°. Second, the 53 and 80 MHz radio images shown in Figure 1 were obtained by subtracting the corresponding radio images obtained ≈ 5 min earlier at the respective frequencies. This time interval is lesser than the period (≈20 min) over which radio source positions at low frequencies usually change due to ionospheric effects (Mercier, 1996; Stewart & McLean, 1982). The brightness temperatures (T_b) of the radio sources shown in Figure 1 near their centroids are $T_b^{80} \approx 3.4 \times 10^5$K (80 MHz) and $T_b^{53} \approx 0.8 \times 10^5$K (53 MHz). The corresponding flux density (S) values are $S_{80} \approx 0.14$sfu (80 MHz) and $S_{53} \approx 0.06$sfu (53 MHz). The spectral index (α) derived from the above flux densities is ≈ 2.1. These are in agreement with that reported for thermal emission from the solar corona at low frequencies (Erickson et al., 1977; Ramesh et al., 2000b, 2006a, 2010a; Sheridan & McLean, 1985; K. R. Subramanian & Sastry, 1988). Furthermore, no nonthermal radio bursts were observed either elsewhere (ftp://ftp.swpc.noaa.gov/pub/warehouse) or with GLOSS or GRASP during the particular observing period. Therefore it is likely that the enhanced radio emission in Figure 1 is thermal in nature. The contrast of such emission is generally better at frequencies <100 MHz (e.g., Lantos et al., 1987). Model calculations by Bastian and Gary (1997) also indicate that it is possible to observe enhanced thermal emission from particularly the off-limb CMEs using different images as in the present case. The above T_b values are reasonably consistent with those predicted by the aforementioned model for thermal emission from a "typical" CME in the same frequency range. Note that for nonthermal gyrosynchrotron emission from a CME, the T_b values predicted by the model are higher than the aforementioned observed T_b values by about a factor of four, even for the lowest values assumed for the different parameters in the model.

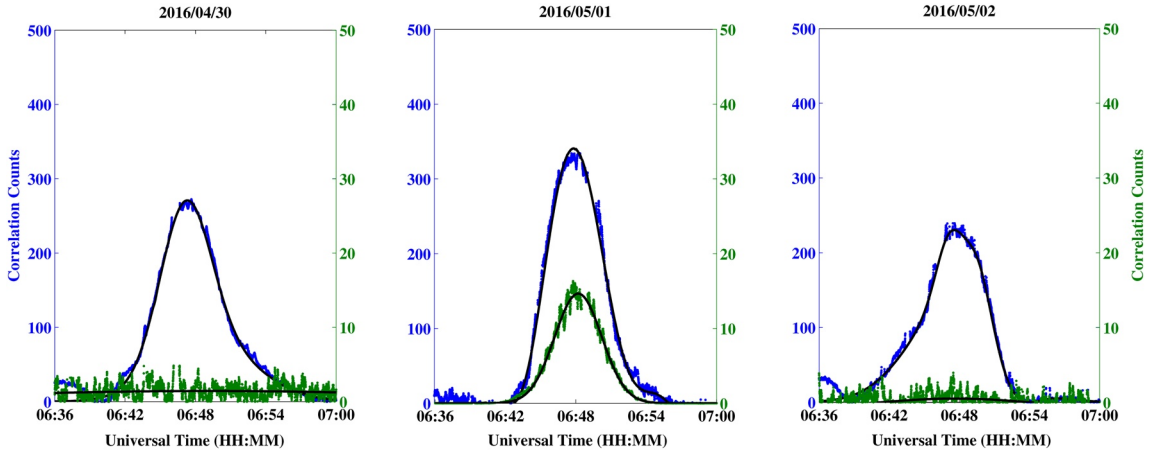

Figure 3. GRIP observations of Stokes I ("blue") and V ("green") emission at 80 MHz in the transit mode around 06:48 UT. The asymmetry in the Stokes I observations on May 2, 2016 was due to a local radio frequency interference (RFI) around ≈ 06:40 UT. The 'solid' lines shown in black color are the "fit" to the respective data points.

Low-frequency observations reported earlier also indicate that the observed T_b of gyro-synchrotron emission from a CME is $\sim 10^7 - 10^8$K (Dulk, 1985; Gary et al., 1985; Gopalswamy & Kundu, 1987, 1990; Sasikumar Raja et al., 2014; Wagner et al., 1981).

Figure 3 shows the GRIP observations in the transit mode at 80 MHz on April 30, May 1, and May 2, 2016 around ≈ 06:48 UT. The half-power width of the response pattern of GRIP at the above frequency is ≈ 1.8°. Since this is wider than the size of the Sun, the observations in Figure 3 correspond to integrated emission from the "whole" Sun at 80 MHz. The gradual increase/decrease in the observed correlation count is due to the passage of the Sun across the response pattern of GRIP. A noticeable Stokes V emission was observed on May 1, 2016, with a peak correlation count of ≈ 15. No similar emission was observed on April 30 and May 2, 2016. The Stokes I emission on May 1, 2016 also shows an increase of ≈ 125 counts as compared to the observations on May 2, 2016 (i.e., from ≈ 225 to ≈ 350 counts). The Sun was "quiet" on April 30, 2016 too, but the peak Stokes I correlation count (≈255) was slightly higher. Following the study by Kundu et al. (1977), we used May 2, 2016 observations as the reference value for "quiet" Sun to estimate the aforementioned increase in the Stokes I correlation count on May 1, 2016. Based on the above, we calculated the degree of circular polarization ($dcp = \frac{|V|}{I}$) for the observations on May 1, 2016, and the value obtained is ≈ 12%. This is lesser than the *dcp* reported for nonthermal gyrosynchrotron radio emission from CME-associated radio emission in a similar frequency range (Dulk, 1985; Sasikumar Raja et al., 2014). The absence of radio bursts during our observing period on May 1, 2016 argues against any nonthermal origin for the observed Stokes V emission (e.g., Mugundhan, Ramesh, Kathiravan, Gireesh, & Hegde, 2018). The possibility of nonthermal noise storm continuum emission too can be ruled out since the sunspot region AR12541 in which there was the activity that day was behind the limb as mentioned earlier and noise storm sources are highly directive (Ramesh et al., 2011). Coincidentally, the GRIP observations on May 1, 2016 were nearly at the same time as the GRAPH observations in Figure 1. One of the observing frequencies with the GRAPH (80 MHz) was also the same as that of the GRIP. Therefore, it is possible that, as observed on 2016 May 1, 2016, Stokes V emission 1 as shown in Figure 3 could be due to the enhanced thermal emission above the limb in Figure 1 at the same frequency (Ramesh, Kathiravan, & Sastry, 2010a; Sastry, 2009). Note that the thermal emission could be circularly polarized in the presence of a magnetic field. Since the medium becomes birefringent due to the latter, the randomly polarized thermal radiation propagates in two orthogonal circular modes, that is, the ordinary ("o") and the extraordinary ("e") mode. A difference between the optical depths and hence the T_b of the two modes will result in a finite value of *dcp*, if the corona is not optically thick.

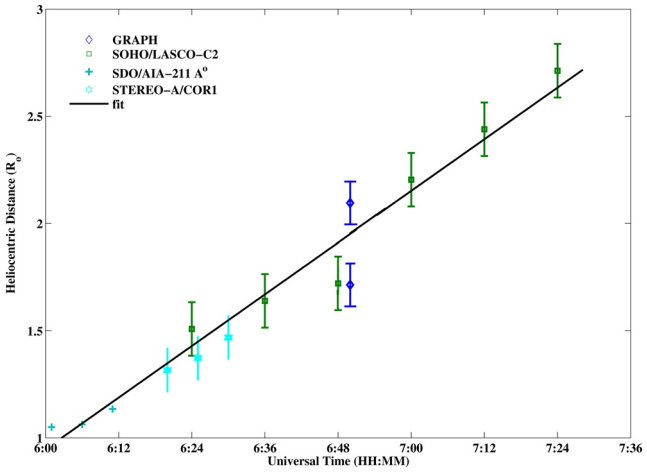

Figure 4. CME h-t plot obtained using EUV, whitelight, and radio observations.

3. Analysis and Results

According to SOHO/LASCO CME catalog, the LE of whitelight CME shown in Figure 1 was at $r_{cme} \approx 3.86$ $R_\odot$ around ≈ 06:48 UT, nearly the same epoch as the GRAPH observations. But the centroids of the radio emission are located at $r_{80} \approx 1.7 \pm 0.2$ $R_\odot$ (80 MHz) and $r_{53} \approx 2.1 \pm 0.2$ $R_\odot$ (53 MHz). Therefore, it is likely that the radio sources are not associated with the LE of the frontal structure in the whitelight CME. They seem to correlate spatially with parts of the frontal structure behind its LE. The separation between the centroids of the 80 and 53 MHz radio sources in Figure 1 suggests a possible density gradient in the frontal structure similar to that in the background corona since it is well known that radio emission from the Sun at a particular frequency (f) can propagate toward the observer only from/above the critical level at which the plasma frequency (f_p) corresponding to the local electron density (N_e) equals f. Note that a gradually increasing N_e (toward the Sunward side) in the CME frontal structure is possible if there is material pile-up from lower coronal levels (Bein et al., 2013; P. Subramanian & Vourlidas, 2007). We generated an h-t plot using centroids of EUV eruptive activity, the frontal structure of whitelight CME, and radio sources (Figure 4). To identify the centroids of EUV and whitelight structures, we fitted each of them with a circumcircle. The LE of the corresponding structure and the solar limb were assumed to be the upper and lower boundaries (e.g., Bein et al., 2013). The h-t measurements obtained with STEREO-A/COR1 were multiplied by 1/cos(24°) to correct for projection effects. All the data points are reasonably well aligned with the linear least squares fit line. The speed of the CME (v_{cme}) estimated from the aforesaid fit is ≈ 233 km/s. Note that since GRAPH observations were confined to 80 and 53 MHz, there are only two data points from GRAPH.

It is known that the larger density gradient near the solar limb leads to the refraction of low-frequency radio waves. So, the contribution to observed thermal bremsstrahlung emission at any given frequency is primarily from regions well above the corresponding plasma level. This implies smaller optical depth (τ) since the absorption coefficient and hence τ are maximum only near the plasma level (e.g., Aubier et al., 1971; Smerd, 1950; Vocks et al., 2018). In the case of the solar corona, T_b and τ are related to its electron temperature ($T_e \approx 10^6$K) as $T_b \approx T_e(1-e^{-\tau})$. Since τ above the limb is small as mentioned, $T_b < T_e$ although the spectral index could be indicative of optically thick thermal emission. The emission from CMEs too undergoes refraction and reflection near the plasma layer as described above (e.g., Bastian & Gary, 1997). The fact that T_b^{80} and T_b^{53} in the present case (see Section 2) are lesser than T_e also indicates the same. Note that since a CME contains primarily coronal material, its T_e is considered to be the same as that of the surrounding corona (e.g., Vourlidas, 2004). Using the aforementioned relation, we calculated τ corresponding to T_b^{80} and T_b^{53}, and the values are $\tau_{80} \approx 0.4$ and $\tau_{53} \approx 0.1$. These are reasonably consistent with τ values for similar frequencies and at locations above the solar limb as in the present work (e.g., Smerd, 1950; Thejappa & Kundu, 1992; Vocks et al., 2018). Based on this, we then estimated N_e at $r_{80} \approx 1.7 \pm 0.2$ $R_\odot$ and $r_{53} \approx 2.1 \pm 0.2$ $R_\odot$ using the relation $\tau = 2 \times 10^{-24} N_e^2 L T_e^{-1.5} f^{-2} \eta^{-1}$, where L (cm) is the width of radio source along the line of sight and $\eta = \sqrt{1 - 80.6 \times 10^6 N_e f^{-2}}$ is the refractive index (e.g., Sheridan & McLean, 1985). The lateral and radial widths of the radio sources shown in Figure 1 are $w_{80} \approx 15 \times 16'$ (80 MHz) and $w_{53} \approx 26 \times 29'$ (53 MHz). Assuming L as the average of lateral and radial widths, we find that $N_e^{80} \approx 2.2 \times 10^7 cm^{-3}$ at $r_{80} \approx 1.7 \pm 0.2$ $R_\odot$ and $N_e^{53} \approx 1.0 \times 10^6 cm^{-3}$ at $r_{53} \approx 2.1 \pm 0.2$ $R_\odot$. These are in good agreement with our independent estimates of CME density using linearly polarized brightness (pB) measurements with STEREO-A/COR1 and the inversion technique based on spherically symmetric polynomial approximation (SSPA; solar.physics.montana.edu/wangtj/sspa.tar; [Wang and Davila, 2014; Wang et al., 2017]). At ≈ 06:50 UT (about the same time as GRAPH observations), we find $N_e^{cor1a} \approx 4.8 \pm 1.4 \times 10^6 cm^{-3}$ near $r \approx 2.1$ $R_\odot$ (see Figure 2).

Considering the coronal plasma as fully ionized gas of normal solar composition (90% hydrogen and 10% helium by number), it can be found that each electron is associated with ~2×10^{-24}g of material. Therefore, the mass of the enhancement is given by $M = 2 \times 10^{-24} N_e V$, where V is the volume of enhance-

ment. We calculated V as $w_{80} \times L_{80}$ and $w_{53} \times L_{53}$ at 80 and 53 MHz, respectively. For N_e at the above two frequencies, we used N_e^{80} and N_e^{53} calculated earlier. Substituting for different values in the above relation, we get $M_{80} \approx 1.3 \times 10^{16}$g (80 MHz) and $M_{53} \approx 3.4 \times 10^{15}$g (53 MHz). The average of the above values is $M_{cme}^{radio} \approx 7.4 \times 10^{15}$g. Using this and v_{cme} mentioned earlier, we calculated the CME kinetic energy $E_{cme}^{radio} \approx 2 \times 10^{30}$erg. The estimates of M_{cme}^{radio} and E_{cme}^{radio} agree reasonably with the mass and kinetic energy of the CME estimated using SOHO/LASCO-C2 observations (see Section 2). Having said so, we would like to mention here that the values of M_{cme}^{radio} and E_{cme}^{radio} calculated above should be considered as upper limits due to lack of information on L. For example, if we assume that L is equal to density scale height in the corona (i.e., $\approx 10^5$ km), then both M_{cme}^{radio} and E_{cme}^{radio} should be lesser by about an order of magnitude. So, the more appropriate results would be $M_{cme}^{radio} \sim 10^{15}$g and $E_{cme}^{radio} \sim 10^{30}$erg. Note that estimates of CME mass using whitelight coronagraph observations too are affected by uncertainities (Bein et al., 2013; Carley et al., 2012; Vourlidas et al., 2000).

Moving to magnetic field strength (b) calculations, Sastry (2009) had shown earlier that if $B \approx 0.5$ G and electron density is $\approx 1.2 \times 10^6$ cm^{-3}, then it should be possible to observe circularly polarized radio emission with $dcp \approx 12\%$. In the present case, the density at $r \approx 2.1$ R$_\odot$ is $\approx 1.0 \times 10^6$ cm$^{-3,}$ and the estimated dcp due to CME associated enhanced radio emission is $\approx 12\%$ as mentioned earlier. Therefore it is likely that magnetic field strength in the CME at the above location is ≈ 0.5 G. This is close to some of the earlier reported B values at nearly the same heliocentric distance from another type of observations like nonthermal gyrosynchrotron emission from the CME loops (Bastian et al., 2001), geometrical properties of the CME flux rope and the shock at its leading edge (Gopalswamy et al., 2012), CME associated fast magnetosonic waves (Kwon et al., 2013), and second harmonic plasma emission from the CME leading edge (Hariharan, Ramesh, Kathiravan, & Wang, 2016). Model calculations reported by Zucca et al. (2014) in connection with a CME-associated coronal type II burst also predict nearly the same value of B at the above r.

4. Summary

We have presented evidence for enhanced thermal radio emission associated with the frontal structure of a CME (from just behind the limb of the Sun) that was observed with SOHO/LASCO-C2 on May 1, 2016. The radio data were obtained with GRAPH at 80 and 53 MHz simultaneously. The plasma characteristics of the CME, estimated from radio observations, are: $N_e \approx 2.2 \times 10^7$ cm^{-3} at $r \approx 1.7$ R$_\odot$ and $N_e \approx 1.0 \times 10^6$ cm^{-3} at $r \approx 2.1$ R$_\odot$; mass and kinetic energy are $\sim 10^{15}$g and $\sim 10^{30}$ erg, respectively; magnetic field strength is $B \approx 0.5$ G at $r \approx 2.1$ R$_\odot$. Future observations with low-frequency radio antenna arrays with larger collecting area like LOFAR and SKA should be able to effectively exploit this possibility for CMEs against the solar disk also (e.g., Ramesh, 2000c).

Data Availability Statement

Data used in the study are at https://www.iiap.res.in/gauribidanur/home.html.

Acknowledgments
The authors thank the staff of Gauribidanur Observatory for their help in the maintenance of antenna, receiver systems, and observations. Ajith Sampath and S. Kokila are thanked for their contributions to the work. The SOHO-LASCO CME catalog is generated and maintained at CDAW Data Center by NASA and the Catholic University of America in cooperation with Naval Research Laboratory. The SDO/AIA data are courtesy of NASA/SDO and AIA science teams. The work of TJW was supported by NASA Cooperative Agreement NNG11PL10 A to CUA and NASA grants 80NSSC18K1131 and 80NSSC18K0668. The authors thank the referee for his/her comments which helped us to present the results in a better manner.

References

Aubier, M., Leblanc, Y., & Boischot, A. (1971). Observations of the 'quiet' sun at decameter wavelengths - Effects of scattering on the brightness distribution. *Astronomy and Astrophysics*, *12*, 435–441.

Aurass, H. (1997). Coronal mass ejections and type II radio bursts. In G. Trottet, (Ed.), Coronal physics from radio and Space observations: Lecture notes in physics (483 (pp. 135–160). https://doi.org/10.1007/BFb0106455

Bain, H. M., Krucker, S., Saint-Hilaire, P., & Raftery, C. L. (2014). Radio imaging of a type IVM radio burst on the 14th of August 2010. *The Astrophysical Journal*, *782*, 43. https://doi.org/10.1088/0004-637X/782/1/43

Bastian, T. S., & Gary, D. E. (1997). On the feasibility of imaging coronal mass ejections at radio wavelengths. *Journal of Geophysical Research*, *102*, 14031–14040. https://doi.org/10.1029/97JA00483

Bastian, T. S., Pick, M., Kerdraon, A., Maia, D., & Vourlidas, A. (2001). The coronal mass ejection of 1998 April 20: Direct imaging at radio wavelengths. *The Astrophysical Journal Letters*, *558*, L65–L69 . https://doi.org/10.1086/323421

Bein, B. M., Temmer, M., Vourlidas, A., Veronig, A. M., & Utz, D. (2013). The height evolution of the "true" coronal mass ejection mass derived From STEREO COR1 and COR2 observations. *The Astrophysical Journal*, *768*, 31. https://doi.org/10.1088/0004-637X/768/1/31

Benz, A. O., Monstein, C., Meyer, H., Manoharan, P. K., Ramesh, R., Altyntsev, A., et al. (2009). A world-wide net of solar radio spectrometers: e-CALLISTO. *Earth Moon Planet*, *104*, 277–285. https://doi.org/10.1007/s11038-008-9267-6.

Brueckner, G. E., Howard, R. A., Koomen, M. J., Korendyke, C. M., Michels, D. J., Moses, J. D., et al. (1995). The large angle spectroscopic coronagraph (LASCO). *Solar Physics*, *162*, 357–402. https://doi.org/10.1007/BF0073343410.1007/978-94-009-0191-9_10

Carley, E. P., James McAteer, R. T., Gallagher, P. T., (2012). Coronal mass ejection mass, energy, and force estimates using STEREO. *The Astrophysical Journal*, *752*, 36. https://doi.org/10.1088/0004-637X/752/1/36
Carley, E. P., Vilmer, N., Simões, P. J. A., & Ó Fearraigh, B. (2017). Estimation of a coronal mass ejection magnetic field strength using radio observations of gyrosynchrotron radiation. *Astronomy and Astrophysics*, *608*, A137. https://doi.org/10.1051/0004-6361/201731368
Chrysaphi, N., Kontar, E. P., Holman, G. D., & Temmer, M. (2018). CME-driven shock and type II solar radio burst band splitting. *The Astrophysical Journal*, *868*, 79. https://doi.org/10.3847/1538-4357/aae9e5
Dulk, G. A. (1985). Radio emission from the sun and stars. *Annual Review of Astronomy and Astrophysics*, *23*, 169–224. https://doi.org/10.1146/annurev.aa.23.090185.001125
Duncan, C. A., Carley, E. P., McCauley, J., & Gallagher, P. T. (2020). Evolution of the Alfv́en Mach number associated with a coronal mass ejection shock. *Astronomy and Astrophysics*, *633*, A56. https://doi.org/10.1051/0004-6361/20173136810.1051/0004-6361/201936449
Ebenezer, E., Ramesh, R., Subramanian, K. R., Sundara Rajan, M. S., & Sastry, C. V. (2001a). A new digital spectrograph for observations of radio burst emission from the Sun. *Astronomy and Astrophysics*, *367*, 1112–1116. https://doi.org/10.1051/0004-636110.1051/0004-6361:20000540
Ebenezer, E., Ramesh, R., Subramanian, K. R., Sundara Rajan, M. S., & Sastry, C. V. (2001b). A new digital spectrograph for observations of radio 329 burst emission from the Sun. *367*, 1112–1116. https://doi.org/10.1051/0004-6361:20000540
Ebenezer, E., Subramanian, K. R., Ramesh, R., Rajan, S. M. S., & Kathiravan, C. (2007). Gauribidanur radio array solar spectrograph. *Bulletin of the Astronomical Society of India*, *35*, 111–119.
Erickson, W. C., Gergely, T. E., Kundu, M. R., & Mahoney, M. J. (1977). Determination of the decameter wavelength spectrum of the quiet Sun. *Solar Physics*, *54*, 57–63. https://doi.org/10.1007/BF00146425
Gallagher, A. (2004). Radio observations of coronal mass ejections. In D. E. Gary, & C. U. Keller, (Eds.), Solar and space weather radio physics: Astrophysics and space science library 314 (pp. 223–242). https://doi.org/10.1007/1-4020-2814-8
Gary, D. E. (2019). Cause and extent of the extreme radio flux density reached by the solar flare of 2006 December 06. *In Proceeding of 2008 Ionospheric Effects Symposium*. eprint arxiv:1901.09262.
Gary, D. E., Dulk, G. A., House, L. L., Illing, R., & Wagner, W. J. (1985). The type IV burst of 1980 June 29, 0233 UT - Harmonic plasma emission? *Astronomy and Astrophysics*, *152*, 42–50.
Gopalswamy, N. (2006). Coronal mass ejections and type II radio bursts. In N. Gopalswamy, R. Mewaldt, & J. Torsti, (Eds.), Solar eruptions and energetic Particles: Geophys. Monograph ser (165 (pp. 207–220). https://doi.org/10.1029/165GM20
Gopalswamy, N., & Kundu, M. R. (1987). Simultaneous radio and white light observations of the 1984 June 27 coronal mass ejection event. *Solar Physics*, *114*, 347–362. https://doi.org/10.1007/BF00167350
Gopalswamy, N., & Kundu, M. R. (1989). Radioheliograph and white-light coronagraph studies of a coronal mass ejection event. *Solar Physics*, *122*, 145–173. https://doi.org/10.1007/BF00162832
Gopalswamy, N., & Kundu, M. R. (1990). Multiple moving magnetic structures in the solar corona. *Solar Physics*, *128*, 377–397. https://doi.org/10.1007/BF00838474
Gopalswamy, N., & Kundu, M. R. (1992). Estimation of the mass of a coronal mass ejection from radio observations. *The Astrophysical Journal*, *390*, L37–L39. https://doi.org/10.1086/186366
Gopalswamy, N., & Kundu, M. R. (1993). Thermal and nonthermal emissions during a coronal mass ejection. *Solar Physics*, *143*, 327–343. https://doi.org/10.1007/BF00646491
Gopalswamy, N., Nitta, N., Akiyama, S., Mäkelä, P., & Yashiro, S. (2012). Coronal magnetic field measurement from Euv images made by the solar dynamics observatory. *The Astrophysical Journal*, *744*, 72. https://doi.org/10.1088/0004-637X/744/1/72
Hariharan, K., Ramesh, R., & Kathiravan, C. (2015). Observations of near-simultaneous split-band solar type-II radio bursts at low frequencies. *Solar Physics*, *290*, 2479–2489. https://doi.org/10.1007/s11207-015-0761-5
Hariharan, K., Ramesh, R., Kathiravan, C., Abhilash, H. N., & Rajalingam, M. (2016). High dynamic range observations of solar coronal transients at low radio frequencies with a spectro-correlator. *The Astrophysical Journal*, *222*, 21. https://doi.org/10.3847/0067-0049/222/2/21
Hariharan, K., Ramesh, R., Kathiravan, C., & Wang, T. J. (2016). Simultaneous near-Sun observations of a moving type IV radio burst and the associated white-light coronal mass ejection. *Solar Physics*, *291*, 1405–1416. https://doi.org/10.1007/s11207-016-0918-x
Howard, R. A., Moses, J. D., Vourlidas, A., Newmark, J. S., Socker, D. G., Plunkett, S. P., et al. (2008). Sun Earth connection coronal and heliospheric investigation (SECCHI). *Space Science Reviews*, *136*, 67–115. https://doi.org/10.1007/s11214-008-9341-4
Kathiravan, C., & Ramesh, R. (2004). Estimation of the three-dimensional space speed of a coronal mass ejection using metric radio data. *The Astrophysical Journal*, *610*, 532–536. https://doi.org/10.1086/421381
Kathiravan, C., & Ramesh, R. (2005). Identification of the source region of a "Halo" coronal mass ejection using meter-wavelength radio data. *The Astrophysical Journal*, *627*, L77–L80. https://doi.org/10.1086/431930
Kathiravan, C., Ramesh, R., Barve, I. V., & Rajalingam, M. (2011). Radio observations of the solar corona during an eclipse. *The Astrophysical Journal*, *730*, 91. https://doi.org/10.1088/0004-637X/730/2/91
Kathiravan, C., Ramesh, R., & Nataraj, H. S. (2007). The post-coronal mass ejection solar atmosphere and radio noise storm activity. *The Astrophysical Journal*, *656*, L37–L40. https://doi.org/10.1086/512013
Kathiravan, C., Ramesh, R., & Subramanian, K. R. (2002). Metric radio observations and ray-tracing analysis of the onset phase of a solar eruptive event. *The Astrophysical Journal*, *567*, L93–L95. https://doi.org/10.1086/339801
Kerdraon, A., Pick, M., Trottet, G., Sawyer, C., Illing, R., Wagner, W., & House, L. (1983). The association of radio noise storm enhancements with the appearance of additional material in the corona. *The Astrophysical Journal*, *265*, L19–L21. https://doi.org/10.1086/183950
Kishore, P., Kathiravan, C., Ramesh, R., Rajalingam, M., & Barve, I. V. (2014). Gauribidanur low-frequency solar spectrograph. *Solar Physics*, *289*, 3995–4005. https://doi.org/10.1007/s11207-014-0539-1
Kishore, P., Ramesh, R., Kathiravan, C., & Rajalingam, M. (2015). A low-frequency radio spectropolarimeter for observations of the solar corona. *Solar Physics*, *290*, 2409–2422. https://doi.org/10.1007/s11207-015-0705-0
Kumari, A., Ramesh, R., Kathiravan, C., & Gopalswamy, N. (2017). New evidence for a coronal mass ejection-driven high frequency type II burst near the Sun. *The Astrophysical Journal*, *843*, 10. https://doi.org/10.3847/1538-4357/aa72e7
Kumari, A., Ramesh, R., Kathiravan, C., & Wang, T. J. (2017). Strength of the solar coronal magnetic field - a comparison of independent estimates using contemporaneous radio and white-light observations. *Solar Physics*, *292*, 161. https://doi.org/10.1007/s11207-017-1180-6
Kumari, A., Ramesh, R., Kathiravan, C., Wang, T. J., & Gopalswamy, N. (2019). Direct estimates of the solar coronal magnetic field using contemporaneous extreme-ultraviolet, radio, and white-light observations. *The Astrophysical Journal*, *881*, 24. https://doi.org/10.3847/1538-4357/ab2adf
Kundu, M. R., Gergely, T. E., & Erickson, W. C. (1977). Observations of the quiet Sun at meter and decameter wavelengths. *Solar Physics*, *53*, 489–496. https://doi.org/10.1007/BF00160291

Kwon, R.-Y., Ofman, L., Olmedo, O., Kramar, M., Davila, J. M., Thompson, B. J., & Cho, K.-S. (2013). Stereoobservations of fast magnetosonic waves in the extended solar corona associated with Eit/euv waves. *The Astrophysical Journal*, *766*, 55. https://doi.org/10.1088/0004-637X/766/1/55

Lantos, P., Alissandrakis, C. E., Gergely, T., & Kundu, M. R. (1987). Quiet Sun and slowly varying component at meter and decameter wavelengths. *Solar Physics*, *112*, 325–340. https://doi.org/10.1007/BF00148787

Lemen, J. R., Title, A. M., Akin, D. J., Boerner, P. F., Chou, C., Drake, J. F., et al. (2012). The atmospheric imaging assembly (AIA) on the solar dynamics observatory (SDO). *Solar Physics*, *275*, 17–40. https://doi.org/10.1007/s11207-011-9776-8

Maia, D. J. F., Gama, R., Mercier, C., Pick, M., Kerdraon, A., & Karlický, M. (2007). The radio-coronal mass ejection event on 2001 April 15. *The Astrophysical Journal*, *660*, 874–881. https://doi.org/10.1086/508011

Mann, G., Classen, T., & Aurass, H. (1995). Characteristics of coronal shock waves and solar type II radio bursts. *Astronomy and Astrophysics*, *295*, 775–781.

Mercier, C. (1996). Some characteristics of atmospheric gravity waves observed by radio-interferometry. *Annals of Geophysics*, *14*, 42–58. https://doi.org/10.1007/s00585-996-0042-6

Mondal, S., Oberoi, D., & Vourlidas, A. (2020). Estimation of the physical parameters of a CME at high coronal heights using low-frequency radio observations. *The Astrophysical Journal*, *893*, 28. https://doi.org/10.3847/1538-4357/ab7fab

Monstein, C., Ramesh, R., & Kathiravan, C. (2007). Radio spectrum measurements at the Gauribidanur observatory. *Bulletin of the Astronomical Society of India*, *35*, 473–480.

Morosan, D. E., Kilpua, E. K. J., Carley, E. P., & Monstein, C. (2019). Variable emission mechanism of a type IV radio burst. *Astronomy and Astrophysics*, *623*, A63. https://doi.org/10.1051/0004-6361/201834510

Mugundhan, V., Hariharan, K., & Ramesh, R. (2017). Solar type IIIb radio bursts as tracers for electron density fluctuations in the corona. *Solar Physics*, *292*, 155. https://doi.org/10.1007/s11207-017-1181-5

Mugundhan, V., Ramesh, R., Barve, I. V., Kathiravan, C., Gireesh, G. V. S., Kharb, P., & Misra, A. (2016). Low-frequency radio observations of the solar corona with arcminute angular resolution: Implications for coronal turbulence and weak energy releases. *The Astrophysical Journal*, *831*, 154. https://doi.org/10.3847/0004-637X/831/2/154

Mugundhan, V., Ramesh, R., Kathiravan, C., Gireesh, G. V. S., & Hegde, A. (2018). Spectropolarimetric observations of solar noise storms at low frequencies. *Solar Physics*, *293*, 41. https://doi.org/10.1007/s11207-018-1260-2

Mugundhan, V., Ramesh, R., Kathiravan, C., Gireesh, G. V. S., Kumari, A., Hariharan, K., & Barve, I. V. (2018a). The first low-frequency radio observations of the solar corona on ≈200 km long interferometer baseline. *The Astrophysical Journal*, *855*, L8. https://doi.org/10.3847/2041-8213/aaaf64

Raja, K. S., Kathiravan, C., Ramesh, R., Rajalingam, M., & Barve, I. V. (2013). Design and performance of a low-frequency cross-polarized log-periodic dipole antenna. *The Astrophysical Journal Series*, *207*(1), 2. https://doi.org/10.1088/0067-0049/207/1/2

Ramesh, R. (2000). The 'halo' CME event Of 23 October 1997: Low frequency radio observations of the pre-event corona. *Solar Physics*, *196*, 213–220. https://doi.org/10.1023/A:1005288115027

Ramesh, R. (2005). Low frequency (30-110 MHz) radio imaging observations of solar coronal mass ejections. In K. P. Dere, J. Wang, & Y. Yan, (Eds.), Coronal and Stellar mass ejections: Proceedings of IAU Symposium, 226 (pp. 83–94). https://doi.org/10.1017/S1743921305000190

Ramesh, R. (2011). Low frequency solar radio astronomy at the Indian Institute of Astrophysics. In A. R. Choudhuri, & D. Banerjee, (Eds.), 1st Asia-Pacific Solar Physics Meeting: Astronomical Society of India Conference Series, 2 (pp. 55–61).

Ramesh, R. (2014). Solar observations at low frequencies with the Gauribidanur radioheliograph. In J. N. Chengalur, & Y. Gupta, (Eds.), Metrewavelength sky: Astronomical Society of India Conference Series 13 (pp. 19–24).

Ramesh, R., Anna Lakshmi, M., Kathiravan, C., Gopalswamy, N., & Umapathy, S. (2012a). The location of solar metric type II radio bursts with respect to the associated coronal mass ejections. *The Astrophysical Journal*, *752*, 107. https://doi.org/10.1088/0004-637X/752/2/107

Ramesh, R., Kathiravan, C., Barve, I. V., & Rajalingam, M. (2012b). High angular resolution radio observations of a coronal mass ejection source region at low frequencies during a solar eclipse. *The Astrophysical Journal*, *744*, 165. https://doi.org/10.1088/0004-637X/744/2/165

Ramesh, R., Kathiravan, C., Kartha, S. S., & Gopalswamy, N. (2010b). Radioheliograph observations of metric type II bursts and the kinematics of coronal mass ejections. *The Astrophysical Journal*, *712*, 188. https://doi.org/10.1088/0004-637X/712/1/188

Ramesh, R., Kathiravan, C., & Sastry, C. V. (2003). Metric radio observations of the evolution of a "Halo" coronal mass ejection close to the sun. *The Astrophysical Journal*, *591*, L163–L166. https://doi.org/10.1086/377162

Ramesh, R., Kathiravan, C., & Sastry, C. V. (2010a). Estimation of magnetic field in the solar coronal streamers through low frequency radio observations. *The Astrophysical Journal*, *711*, 1029–1032. https://doi.org/10.1088/0004-637X/711/2/1029

Ramesh, R., Kathiravan, C., & Satya Narayanan, A. (2011). Low-frequency Observations of Polarized Emission from Long-lived Non-thermal Radio Sources in the Solar Corona. *The Astrophysical Journal*, *734*, 39. https://doi.org/10.1088/0004-637X/734/1/39

Ramesh, R., Kathiravan, C., SundaraRajan, M. S., SastryBarve, C. V., & Sastry, C. V. (2008). A low-frequency (30 - 110 MHz) antenna system for observations of polarized radio emission from the solar corona. *Solar Physics*, *253*, 319–327. https://doi.org/10.1007/s11207-008-9272-y

Ramesh, R., Kishore, P., Mulay, S. M., Barve, I. V., Kathiravan, C., & Wang, T. J. (2013). Low-frequency observations of drifting, non-thermal continuum Radio emission associated with the solar Coronal mass ejections. *The Astrophysical Journal*, *778*, 30. https://doi.org/10.1088/0004-637X/778/1/30

Ramesh, R., Kumari, A., Kathiravan, C., Ketaki, D., Rajesh, M., & Vrunda, M. (2020). Low-frequency radio observations of the "quiet" corona during the descending phase of sunspot cycle 24. *Geophysical Research Letters*, *47*, e2020GL090426. https://doi.org/10.1029/2020GL090426

Ramesh, R., Nataraj, H. S., Kathiravan, C., & Sastry, C. V. (2006a). The equatorial background solar corona during solar minimum. *The Astrophysical Journal*, *648*, 707–711. https://doi.org/10.1086/505677

Ramesh, R., Rajan, M. S. S., & Sastry, C. V. (2006b). The 1024 channel digital correlator receiver of the Gauribidanur radioheliograph. *Experimental Astronomy*, *21*, 31–40. https://doi.org/10.1007/s10686-006-9065-y

Ramesh, R., & Sastry, C. V. (2005b). Low frequency (<100 MHz) thermal radio emission from the solar corona and the effect of radial magnetic field. In K. Sankarasubramanian, M. Penn, & A. Pevtsov, (Eds.), Large-scale structures and their role in solar activity: ASP Conference Series, 346 (pp. 153–158).

Ramesh, R., Subramanian, K. R., & Sastry, C. V. (1999a). Eclipse observations of compact sources in the outer solar corona. *Solar Physics*, *185*, 77–85. https://doi.org/10.1023/A:1005149830652

Ramesh, R., Subramanian, K. R., & Sastry, C. V. (1999b). Phase calibration scheme for a "T" array. *Astronomy and Astrophysics Supplementary*, *139*, 179–181. https://doi.org/10.1051/aas:1999387

Ramesh, R., Subramanian, K. R., & Sastry, C. V. (2000b). Estimation of the altitude and electron density of a discrete source in the outer solar corona through low frequency radio observations. *Astrophyics Letters & Communications*, *40*, 93–102.

Ramesh, R., Subramanian, K. R., SundaraRajan, M. S., & Sastry, C. V. (1998). The Gauribidanur radioheliograph. *Solar Physics*, *181*(2), 439–453. https://doi.org/10.1023/A:1005075003370

Ramesh, R., & Sundaram, G. A. S. (2000a). Type I radio bursts and the minimum between sunspot cycles 22 & 23. *Astronomy and Astrophysics*, *364*, 873.

Sasikumar Raja, K., Ingale, M., Ramesh, R., Subramanian, P., Manoharan, P. K., & Janardhan, P. (2016). Amplitude of solar wind density turbulence from 10 to 45 R ⊙. *Journal of Geophysics Research Space Physics*, *121*, 605–611. https://doi.org/10.1002/2016JA023254

Sasikumar Raja, K., & Ramesh, R. (2013). Low-frequency observations of transient quasi-periodic radio emission from the solar atmosphere. *The Astrophysical Journal*, *775*, 38. https://doi.org/10.1088/0004-637X/775/1/38

Sasikumar Raja, K., Ramesh, R., Hariharan, K., Kathiravan, C., & Wang, T. J. (2014). An estimate of the magnetic field strength associated with a solar coronal mass ejection from low frequency radio observations. *The Astrophysical Journal*, *796*, 56. https://doi.org/10.1088/0004-637X/796/1/56

Sastry, C. V. (2009). Polarization of the thermal radio emission from outer solar corona. *The Astrophysical Journal*, *697*, 1934–1939. https://doi.org/10.1088/0004-637X/697/2/1934

Sheridan, K. V., Jackson, B. V., McLean, D. J., & Dulk, G. A. (1978). Radio observations of a massive, slow-moving ejection of coronal material. *PASA: Publications of the Astronomical Society of Australia*, *3*, 249–250. https://doi.org/10.1017/s1323358000015423

Sheridan, K. V., & McLean, D. J. (1985). The 'quiet' sun at meter wavelengths. In D. J. McLean, & N. R. Labrum, (Eds.), *Solar radiophysics: Study of emission from the sun at meter wavelength* (pp. 443–466).

Smerd, S. (1950). Radio-frequency radiation from the quiet sun. *Australian Journal of Chemistry*, *3*, 34–59. https://doi.org/10.1071/PH50003410.1071/ch9500034

Stewart, R. T., McCabe, M. K., Koomen, M. J., Hansen, R. T., & Dulk, G. A. (1974). Observations of coronal disturbances from 1 to 9 $R_{\odot}$. *Solar Physics*, *36*, 203–217. https://doi.org/10.1007/BF00151561

Stewart, R. T., & McLean, D. J. (1982). Correcting low-frequency solar radio source positions for ionospheric refraction. *Publications of the Astronomical Society of Australia*, *4*, 386–389. https://doi.org/10.1017/s1323358000021226

Subramanian, K. R., & Sastry, C. V. (1988). The low-frequency radio spectrum of the continuum emission from the undisturbed sun. *Journal of Astrophysics & Astronomy*, *9*, 225–229. https://doi.org/10.1007/BF02715067

Subramanian, P., & Vourlidas, A. (2007). Energetics of solar coronal mass ejections. *Astronomy & Astrophysics*, *467*, 685–693. https://doi.org/10.1051/0004-6361:20066770

Thejappa, G., & Kundu, M. R. (1992). Unusually low coronal radio emission at the solar minimum. *Solar Physics*, *140*, 19–39. https://doi.org/10.1086/52883510.1007/bf00148427

Tun, S. D., & Vourlidas, A. (2013). Derivation of the magnetic field in a coronal mass ejection core via multi-frequency radio imaging. *The Astrophysical Journal*, *766*, 130. https://doi.org/10.1088/0004-637X/766/2/130

Vasanth, V., Chen, Y., Lv, M., Ning, H., Li, C., Feng, S., et al. (2019). Source imaging of a moving type IV solar radio burst and its role in tracking coronal mass ejection from the inner to the outer corona. *The Astrophysical Journal*, *870*, 30. https://doi.org/10.3847/1538-4357/aaeffd

Vocks, C., Mann, G., Breitling, F., Bisi, M. M., Dabrowski, B., Fallows, R., et al. (2018). LOFAR observations of the 'quiet' solar corona. *Astronomy & Astrophysics*, *614*, A54. https://doi.org/10.1051/0004-6361/201630067

Vourlidas, A., Howard, R. A., Esfandiari, E., Patsourakos, S., Yashiro, S., & Michalek, G. (2010). Comprehensive analysis of coronal mass ejection mass and energy properties over a full solar cycle. *The Astrophysical Journal*, *722*, 1522–1538. https://doi.org/10.1088/0004-637X/722/2/1522

Vourlidas, A., Subramanian, P., Dere, K. P., & Howard, R. A. (2000). Large-angle spectrometric coronagraph measurements of the energetics of coronal mass ejections. *The Astrophysical Journal*, *534*, 456–467. https://doi.org/10.1086/308747

Wagner, W. J., Hildner, E., House, L. L., Sawyer, C., Sheridan, K. V., & Dulk, G. A. (1981). Radio and visible light observations of matter ejected from the Sun. *The Astrophysical Journal*, *244*, L123–L126. https://doi.org/10.1086/183495

Wang, T., & Davila, J. M. (2014). Validation of spherically symmetric inversion by use of a tomographically reconstructed three-dimensional electron density of the solar corona. *Solar Physics*, *289*, 3723–3745. https://doi.org/10.1007/s11207-014-0556-0

Wang, T., Reginald, N. L., Davila, J. M., St Cyr, O. C., & Thompson, W. T. (2017). Variation in coronal activity from solar cycle 24 minimum to maximum using three-dimensional reconstructions of the coronal electron density from STEREO/COR1. *Solar Physics*, *292*, 97. https://doi.org/10.1007/s11207-017-1130-3

Wu, C., Mann, G., Breitling, F., Bisi, M. M., Dąbrowski, B., Fallows, R., et al. (2018). LOFAR observations of the quiet solar corona. *Astronomy and Astrophysics*, *614*, A54. https://doi.org/10.1051/0004-6361/201630067

Zucca, P., Pick, M., Démoulin, P., Kerdraon, A., Lecacheux, A., & Gallagher, P. T. (2014). Understanding coronal mass ejections and associated shocks in the solar corona by merging multiwavelength observations. *The Astrophysical Journal*, *795*, 68. https://doi.org/10.1088/0004-637X/795/1/68